Earth and Planetary Science Letters 525 (2019) 115733

Contents lists available at ScienceDirect

Earth and Planetary Science Letters

www.elsevier.com/locate/epsl

On the role of chemical weathering of continental arcs in long-term climate regulation: A case study of the Peninsular Ranges batholith, California (USA)

Hehe Jiang*, Cin-Ty A. Lee

Department of Earth, Environmental and Planetary Sciences, Rice University, Houston, TX, United States

ARTICLE INFO

Article history:
Received 9 November 2018
Received in revised form 11 July 2019
Accepted 26 July 2019
Available online 16 August 2019
Editor: A. Yin

Keywords:
continental arc
silicate weathering
long-term carbon cycle
feedback strength
Peninsular Ranges

ABSTRACT

The long-term stability of atmospheric pCO_2 is dominantly determined by the balance between the rate of CO_2 input from magmatic/metamorphic degassing and the efficiency of CO_2 uptake by silicate weathering via eventual precipitation as marine carbonate and by organic carbon burial. Silicate weathering is thought to represent a negative feedback to changes in atmospheric pCO_2. The Late Cretaceous-Early Cenozoic was characterized by elevated atmospheric pCO_2 and greenhouse climate, widely thought to be due to increased magmatic flux from mid-ocean ridges, flood basalts and continental arcs. Of interest here is the role of continental arcs in modulating long term atmospheric CO_2 contents and climate. Continental arc magmatism is accompanied by rapid uplift and erosion due to magmatic/tectonic thickening of the crust, thus, the development of continental arcs might also enhance the global efficiency of silicate weathering, in turn increasing the efficiency of carbon sequestration. To assess the contribution of continental arcs to global carbon sinks, we conducted a case study in the Cretaceous Peninsular Ranges batholith (PRB) and associated forearc basin in southern California, USA, representing one segment of a Mesozoic circum-Pacific continental arc system. Arc magmatism occurred between 170-85 Ma, peaking at 100 Ma. Erosion occurred during magmatism and continued well into the early Eocene, with forearc sediments representing the products of this protracted unroofing of the arc. By calculating the depletion of Ca in forearc sediments relative to their arc protoliths, we estimate chemical weathering fluxes (in equivalent CO_2) to be $\sim 10^6$ mol km^{-2} yr^{-1} near the end of magmatism, decreasing to $\sim 10^5$ mol km^{-2} yr^{-1} by the Early Eocene. Integrated over the entire magmatic and post-magmatic history of the batholith, the total amount of CO_2 consumed through chemical weathering is comparable to that degassed. However, during magmatism, the regional degassing flux exceeds the regional weathering flux even though the efficiency of weathering is increased due to magmatic and tectonic uplift. After magmatism ends, continued erosion from remnant topography causes the arc to transition into a net regional sink, increasing the global efficiency of chemical weathering and amplifying cooling after magmatism ends. Understanding how atmospheric CO_2 and climate vary over long timescales requires an understanding of how magmatic orogenies enhance degassing but also increase the strength of the global silicate weathering feedback.

1. Introduction

The long-term variability of atmospheric-oceanic pCO_2 is largely determined by the balance between the rate of geologic inputs of CO_2 through magmatic/metamorphic degassing and the rate of carbonate precipitation driven by silicate weathering and the rate of organic carbon burial (Berner, 1991; Kump and Arthur, 1999). Due to the small size of the surface carbon reservoir relative to the inputs to and from the solid Earth, a negative feedback between silicate weathering and climate is thought to be required for a stable climate system (Walker et al., 1981; Berner and Caldeira, 1997). This feedback stabilizes atmospheric CO_2 on timescales of 10^5 to 10^6 yr (Sundquist, 1991; Berner and Caldeira, 1997; Zeebe, 2012). As a result, over million year timescales, global CO_2 inputs into and outputs from the ocean-atmosphere (exogenic) system is generally considered to be balanced (Berner, 1991; Kump and Arthur, 1999). The steady state pCO_2 level is thus determined by the input and the strength of the silicate weathering feedback, which reflects the efficiency of silicate weathering in

* Corresponding author.
E-mail address: jiang.hehe0518@gmail.com (H. Jiang).

https://doi.org/10.1016/j.epsl.2019.115733
0012-821X/

drawing down atmospheric CO_2 (Walker et al., 1981; Brady, 1991; Berner, 1994; Caves et al., 2016). Long term carbon inputs are primarily from volcanic/metamorphic degassing through mid-ocean ridges, volcanic arcs in subduction zones, and large igneous provinces (Berner, 1991; Lee et al., 2013). Feedback strength is controlled by erosional supply and dissolution kinetics, which are influenced by lithology and hydrologic conditions (West et al., 2005; Maher and Chamberlain, 2014; Jagoutz et al., 2016). Over geologic history, Earth has experienced several profound long-term climate transitions, which appear to also reflect changes in the baseline CO_2 content of the exogenic system (Berner, 1991; Zachos et al., 2008; Park and Royer, 2011). These changes are driven by changes in input or the efficiency of the global weathering feedback.

Because variability in the long-term carbon cycle is controlled by interactions between the surface and solid Earth, the question arises as to how tectonism modulates both carbon inputs and sink efficiency. There has been recent interest in the role of continental magmatic arcs in modulating long-term climate, such as during the Cretaceous greenhouse (Lee et al., 2013; Mckenzie et al., 2014; Lee et al., 2015). During the Cretaceous, the total length of continental arcs appears to have been twice that of the present day due to development of a circum-Pacific chain of continental arcs (Lee et al., 2013; Cao et al., 2017). In particular, many of the arcs intersected ancient sedimentary carbonates stored in the overlying continental plate, leading to the hypothesis that continental arc activity may have increased global CO_2 production by 3-5 times relative to the late Cenozoic (Lee et al., 2013). However, with high magmatic addition accompanied by crustal thickening, continental arcs also become the locus of rapid uplift and erosion (Kimbrough et al., 2001; Lee et al., 2015; Jiang and Lee, 2017), begging the question if the arcs themselves also increase weathering efficiency. The key issue is thus to address whether magmatic orogens serve as a net carbon source or a net sink.

We conducted a case study of forearc sediments derived from a segment of the Cretaceous Cordilleran arc and established a method for constraining regional chemical weathering flux (in equivalent CO_2) based on the geochemistry of source rock and erosional products. Our results suggest high chemical weathering flux during arc unroofing due to high denudation rate. We also estimated regional carbon fluxes based on published magmatic addition rates (Jiang and Lee, 2017) and chemical weathering fluxes from this study. We show that the arc served as a net carbon source during the Late Cretaceous magmatic flare-up, but transitioned into a regional carbon sink in the Early Cenozoic as erosion continued after arc magmatism terminated. The development of continental arcs increases weatherability through mountain building processes, enhancing the negative global feedback. Whether continental arcs serve as a net regional input or output of CO_2 depends on the interplay between magmatic inputs and weathering, which changes throughout the "lifespan" of an arc.

2. The Peninsular Ranges batholith and associated forearc basin

The northern Peninsular Ranges batholith (PRB) is one segment of the Mesozoic Cordilleran arc, which developed along the western margin of the Precambrian North American craton by subduction of the Farallon oceanic plate beneath the North America continent. The PRB is composed of mostly Cretaceous plutonic rocks, which intruded into the Early Cretaceous Santiago Peak volcanic and Paleozoic-Jurassic metasedimentary rocks (Fig. 1). The plutonic rocks range from gabbroic to granitic compositions (Todd et al., 1988; Lee et al., 2007; Morton et al., 2014). The batholith was emplaced between 170 and 85 Ma, among which the 100-90 Ma La Posta-type plutons comprise more than 40% of the northern PRB (Morton et al., 2014).

Rapid unroofing of the PRB took place during the Late Cretaceous-early Eocene, shortly after the emplacement of the La Posta-type plutons, resulting in the development of a forearc sedimentary sequence along the western PRB within the Santa Ana Mountains-San Diego area. Previous petrographic studies suggest that the Upper Cretaceous–Paleocene/Lower Eocene sediments contain significant amounts of plutonic materials (Schoellhamer et al., 1981; Girty, 1987). Over 90% of the detrital zircons from these sediments have U–Pb ages falling within the age range of Peninsular Ranges plutonic rocks, suggesting a major batholithic source (Sharman et al., 2015; Jiang and Lee, 2017) (Fig. 2). During this period, the PRB was likely characterized by high relief and became a topographic barrier to external sedimentary sources. In comparison, Late Eocene sediments have zircon populations with Paleozoic and Precambrian ages, suggesting that the topographic high of the PRB had been removed, allowing for the introduction of sediments of continental provenance further east (Sharman et al., 2015; Jiang and Lee, 2017) (Figs. 1, 2).

The PRB was characterized by high magmatic addition and denudation rates during the Late Cretaceous-early Eocene of approximately 0.1–2 $km^3/km^2/Myr$ (Grove et al., 2003; Jiang and Lee, 2017). Magmatic addition peaked at 100–90 Ma, followed by a protracted period of decreasing erosion rates between 90–50 Ma. The magmatic addition/denudation rate estimates and detrital zircon signals suggest that development of the PRB was accompanied by mountain building (Kimbrough et al., 2001; Jiang and Lee, 2017). Up to 5 km elevation increase during the Late Cretaceous magmatic flare-up has been estimated (Jiang and Lee, 2017). Magmatic thickening triggered uplift and rapid erosion, which resulted in gradual smoothing of the topography and exhumational thinning of the crust by late Eocene time (Jiang and Lee, 2017).

3. Approach

Given that most Late Cretaceous–Early Eocene sediments were sourced from PRB plutons, the difference in chemical composition between the arc rocks and forearc sediments represents the total chemical weathering flux integrated over residence in the soil mantle and during erosion, transport and deposition of the exhumed arc rocks. The flux of elemental loss can then be converted into CO_2 consumption during arc exhumation. Quantifying elemental loss/gain, however, requires an estimate of the average protolith composition. Below, we outline how to reconstruct protolith compositions and estimate weathering losses.

3.1. Chemical depletion fraction and weathering flux

For a weathering zone with steady state thickness, total denudation mass flux (D) is a sum of physical weathering (E) and chemical weathering mass fluxes (W) (tons/km^2/yr) (Nesbitt, 1979; Riebe et al., 2003) (Fig. 3):

$$D = W + E \tag{1}$$

For any mobile element X (e.g. Ca, Mg, etc.), the mass balance relation is:

$$D \cdot [\mathrm{X}]_P = W_x + E \cdot [\mathrm{X}]_S \tag{2}$$

where $[X]_p$ and $[X]_s$ is the concentration of element X in the parent rock and erosional product, respectively. In our case, the parent is the PRB plutonic rocks, and the erosional product is the Upper Cretaceous–Lower Eocene sediments. $D \cdot [X]_P$ represents the rate of fresh material supply (e.g., bedrock to soil conversion rate), and W_x is the chemical weathering flux of element X. For an immobile element I (e.g. Zr, Ti, etc.) (Brimhall and Dietrich, 1987;

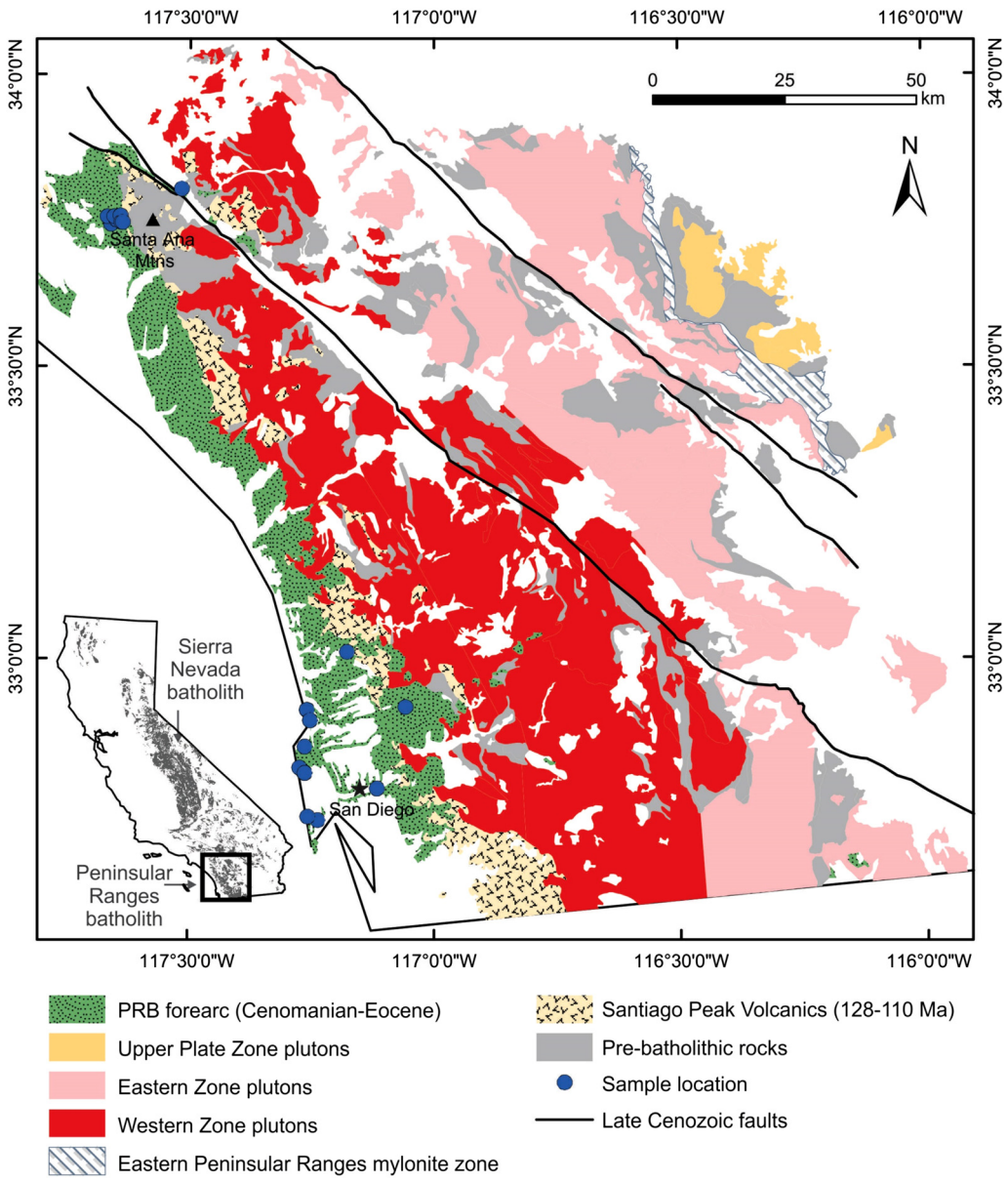

Fig. 1. Geologic map of the northern Peninsular Ranges batholith (PRB) and associated forearc basin sediments (modified after Sharman et al. (2015) and Jiang and Lee (2017).

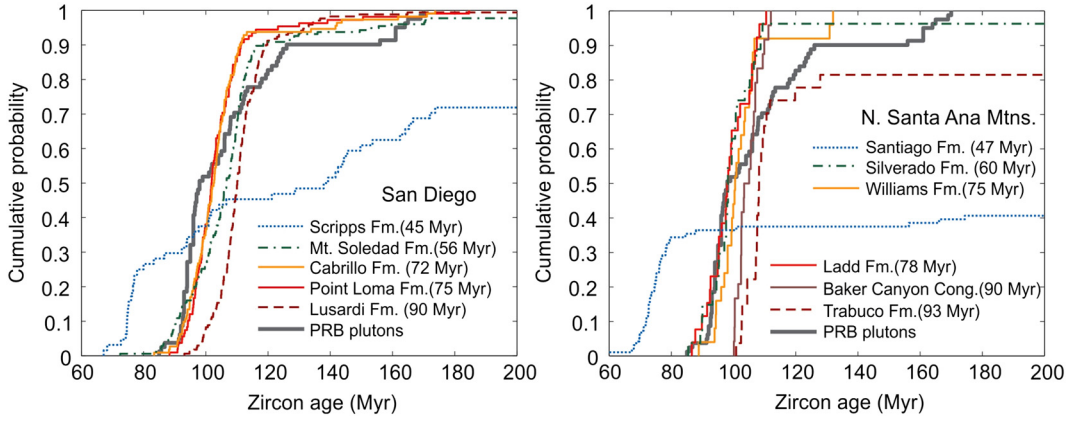

Fig. 2. Cumulative probability plots for zircon U–Pb ages for the Cretaceous PRB plutons and Upper Cretaceous–Early Eocene forearc strata in San Diego and the northern Santa Ana Mountains. Detrital zircon ages in the Upper Cretaceous to Lower Eocene (in San Diego) or Paleocene (in Santa Ana Mountains) are consistent with those in the PRB plutons. However, detrital zircons in the Upper Eocene sediments contain significant amounts of younger grains, suggesting a provenance different from the PRB due to removal of the topographic barrier in the PRB. Zircon ages in the PRB plutons are from Walawender et al. (1990), Thomson and Girty (1994), Shaw et al. (2003) and Premo et al. (2014). Detrital zircon ages in forearc sediments are from Sharman et al. (2015) and Jiang and Lee (2017).

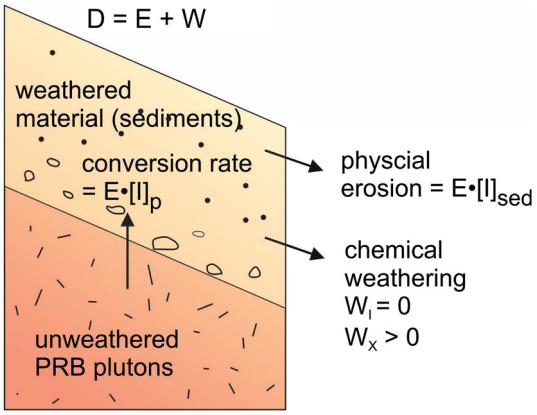

Fig. 3. Schematic diagram showing the mass balance of mobile and immobile elements during weathering of arc rocks. Modified after Riebe et al. (2003) and Lee et al. (2015).

Middelburg et al., 1988), chemical weathering flux is close to zero and Eq. (2) becomes

$$D \cdot [\mathrm{I}]_P = E \cdot [\mathrm{I}]_S \tag{3}$$

The chemical depletion fraction of an individual mobile element can be calculated as

$$CDF_x = \frac{W_x}{D[X]_P} = 1 - \frac{[\mathrm{X}]_S/[\mathrm{I}]_S}{[\mathrm{X}]_P/[\mathrm{I}]_P} \tag{4}$$

where CDF_x is the fraction of element X lost through chemical weathering compared to its concentration in the parent rock; CDF_x when summed over all elements is a measure of the intensity of chemical weathering. It follows that the chemical weathering flux of element X is

$$W_x = D \cdot [\mathrm{X}]_P \cdot CDF_x \tag{5}$$

For sedimentary rocks, the challenge is to obtain the parent rock composition $[\mathrm{X}]_P$ and $[\mathrm{X}]_P/[\mathrm{I}]_P$. Assuming immobile element ratios are not affected by weathering processes, we can use immobile element ratios in sediments to reconstruct the parent rock composition ($[\mathrm{I}_1]_S/[\mathrm{I}_2]_S = [\mathrm{I}_1]_P/[\mathrm{I}_2]_P$) (Nesbitt, 1979). The ideal immobile element ratios are those that involve elements, which are fractionated during magmatism, but not during weathering. For example, Zr and Ti are relatively immobile during chemical weathering. In the PRB plutonic rocks, Zr increases and Ti decreases with increasing silica content from gabbroic to granitic compositions. This is because Ti is removed early by magnetite Fe–Ti oxide fractionation, while Zr remains as an incompatible element and thus increases until late stage zircon saturation (Lee and Bachmann, 2014). We find that there are systematic monotonic positive or negative correlations between major elements (e.g., Si, Ca, Mg, Na, P, etc.) and Ti/Zr during magmatic differentiation. By normalizing all elements to immobile Zr, we can use these elemental ratios to calculate the chemical weathering fraction and flux.

While immobile element ratios should not change significantly during chemical weathering, there is the possibility for physical fractionation during sedimentary transport. Immobile elements are often associated with heavy minerals, such as magnetite, ilmenite, titanite, and zircon, making them prone to any processes involving sorting of grains by buoyancy. These concerns will be addressed in the results section.

3.2. Cation fluxes and CO_2 consumption

On geological timescales, removal of atmospheric CO_2 is largely controlled by dissolution of calcsilicates:

$$2CO_2 + 3H_2O + CaSiO_3 \rightarrow H_4SiO_4 + Ca^{2+} + 2HCO_3^- \tag{6}$$

$$2HCO_3^- + Ca^{2+} \rightarrow CaCO_3 + CO_2 + H_2O \tag{7}$$

which approximates terrestrial weathering of Ca-bearing silicate rocks followed by the deposition of carbonate (Brady, 1991). Two moles of CO_2 are removed in weathering of calcsilicates, and one mole of CO_2 is released back to the atmosphere after formation of marine carbonates. Release of Mg from silicate rocks during weathering also leads to carbonate deposition following the exchange of Mg for Ca on contact with ocean-floor basalts (Holland, 1984).

Na and K silicates are also involved in silicate weathering, but they are involved in "reverse weathering" reactions in seawater, leading to the formation of Na and K silicates and conversion of HCO_3^- to CO_2 that returns to the atmosphere; this results in a much less control of atmospheric CO_2 by the weathering of Na and K silicate minerals (Berner et al., 1983; Gaillardet et al., 1999). Carbonate weathering consumes CO_2, but the same amount of CO_2 is released back upon carbonate precipitation in the ocean on timescales much shorter than 10^6 years (Berner et al., 1983; Brady, 1991). Therefore, for the long term carbon cycle, we consider silicate weathering of Ca and Mg silicates as the primary net CO_2 drawdown, with one mole of Ca^{2+} and Mg^{2+} released from rock corresponding to one mole of CO_2 consumed from the atmosphere during carbonate precipitation (Gaillardet et al., 1999).

4. Samples and analytical methods

We collected mudstones and sandstones from the Upper Cretaceous–Lower Eocene forearc basin around San Diego and the Northern Santa Ana Mountains in southern California (Fig. 1). These sediments were deposited in submarine fan or fluvial environments (detailed stratigraphy is summarized in Jiang and Lee (2017)), and consist of angular to sub-angular, poorly to moderately sorted framework grains with clay matrix or calcite cement. Samples from San Diego are composed of 30–50% quartz, 40–60% feldspar and ~10% plutonic lithic clasts. Samples from the Santa Ana Mountains contain higher amounts of quartz (up to 60%) and less feldspar.

Seventeen samples were crushed to fine powders in a ceramic mill and fused with lithium tetraborate mix. Bulk chemical compositions were measured by X-ray Fluorescence at Washington State University Peter Hooper GeoAnalytical Lab following methods described in Johnson et al. (1999). Loss on ignition on these samples were also measured in the same lab. Final concentrations of major and trace elements were normalized to 100% volatile-free content (supplementary Table S1).

Most samples collected from San Diego contain variable amounts of carbonate detrital grains or cement (up to 40% by volume), introducing excess Ca to the samples. Since the Ca concentration used to calculate CDF_{Ca} pertains to silicates only, correction for carbonate is needed. To estimate the carbonate proportion in the sandstone, we conducted elemental mapping of the samples using a Horiba XGT-7200 X-ray analytical microscope at Rice University. Elemental mapping was done for major elements under full vacuum with 50 kV accelerating voltage, 1 mA current, 50 µm capillary, 400 s survey time per-frame, and 5 accumulations. Area proportion of carbonate was determined by the areal proportion of pixels with high Ca intensity in the elemental map. For grain-supported samples with small amounts of carbonate, we set the threshold for Ca to be ≥3 counts per second, and for cement-rich samples, the threshold was set at Ca ≥4 counts per second. We also estimated porosity through the proportion of pixels with zero intensity in a composited Si + Al + Fe + K + Ca + Ti + Zr map. We assume area proportion translates into volume proportion, and made a density correction to convert volume proportion to mass proportion, using 2.71 g/cm^3 for pure carbonate and 2.65 g/cm^3

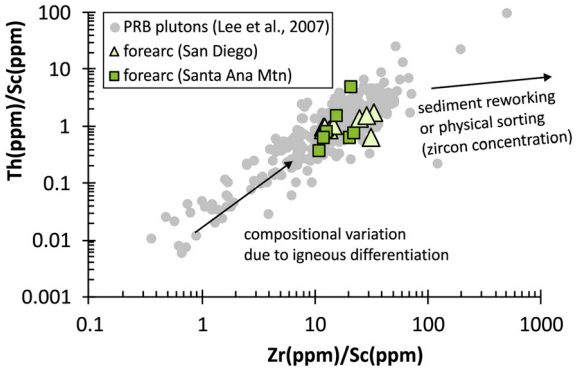

Fig. 4. Zr/Sc vs. Th/Sc diagram showing effect of physical sorting on immobile element ratios. All Upper Cretaceous–Lower Eocene sedimentary rocks have a PRB plutonic composition in terms of immobile element ratios. These immobile element ratios appear not to have been fractionated by physical sorting during sedimentary transport from source to sink.

for silicate minerals from granites (Manger, 1963), but this density correction is essentially negligible. We subtract the Ca in carbonate from the bulk rock Ca concentration assuming all the carbonate is $CaCO_3$ (supplementary Table S2). Carbonate content is negligible in the Santa Ana Mountain samples.

5. Results

5.1. Chemical weathering and physical sorting in the PRB forearc sediments

In Figs. 4–6, we compare element systematics between the forearc sediments and the PRB plutonic rocks. Bulk rock composition of the prebatholithic metasediments (Paleozoic to mid-Mesozoic) (Shaw et al., 2003), Santiago Peak volcanic (Herzig and Kimbrogh, 2014), and sediments from the Late Jurassic forearc (Kimbrough et al., 2014) are also included.

Immobile element ratios can be used to evaluate provenance and the effect of physical sorting. In igneous systems, the ratio of incompatible to compatible elements such as Th/Sc and Zr/Sc, serve as sensitive indices of magmatic differentiation. Th, Zr, and Sc, in particular, are relatively insoluble, thus are transported quantitatively in the terrigenous component of sediment. Among these elements, Th and Sc are considered to be the most useful for source compositions because they are not significantly affected by secondary processes, such as diagenesis and metamorphism, and they are also less affected by heavy mineral sorting during sedimentary processes (Taylor and McClennan, 1985). Zr, however, is controlled by zircon, which is a heavy mineral. Physical sorting in sediments can potentially fractionate Zr/Sc, but not Th/Sc (Taylor and McClennan, 1985; Bahlburg and Dobrzinski, 2011). In Fig. 4, we plot Th/Sc versus Zr/Sc. It can be seen that PRB forearc sediments all cluster within the compositional array defined by the PRB plutons. This suggests that the forearc sediments are primary erosional products from the PRB and that physical sorting did not significantly alter the relative proportions of immobile elements during sedimentation.

The Al_2O_3–CaO + Na_2O–K_2O (A–CN–K) diagram and the chemical index of alteration (CIA = $Al_2O_3/(Al_2O_3 + CaO + K_2O + Na_2O)$*100, in molar fraction) have been used to evaluate chemical weathering intensity (Nesbitt and Young, 1984; Bahlburg and Dobrzinski, 2011) (Fig. 5a). On the A–CN–K diagram (Fig. 5), as weathering progresses, clay minerals are produced at the expense of feldspars, and the bulk compositions of weathering products evolve along the weathering trend (Fig. 5b). Ca, Na and K are leached in preference to Al, thus the most intensely weathered samples plot at the Al-apex on the diagram. The slope of predicted and observed chemical weathering trends is subparallel to the A–CN boundary because plagioclase is more susceptible to weathering than K-feldspar (Nesbitt and Young, 1984). As a result, Ca and Na are leached preferentially over K. The trend intersects the A–K boundary once all plagioclase is weathered, and then is redirected toward the A apex because K is preferentially extracted from the residues. In contrast, physical sorting of the sediments primarily results in enrichment or depletion in relative clay mineral content, without preferential selection of different types of feldspar. The sorting trend on A-CN-K diagram is indicated by the dashed arrows in Fig. 5b. The orientation of the arrows is obtained by projecting a line from the A apex through the point representing the bulk weathering product (green square) and toward the feldspar join (Nesbitt et al., 1996).

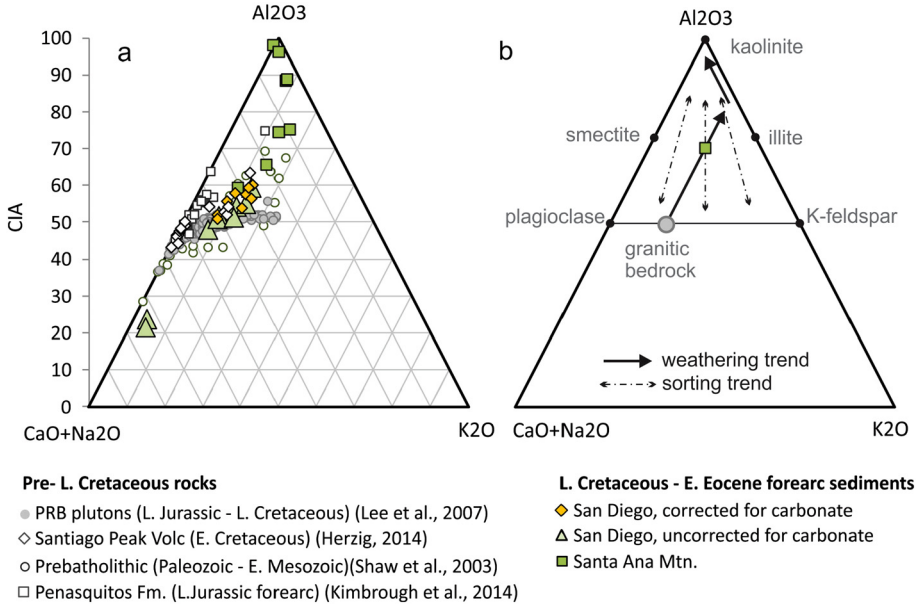

Fig. 5. A–CN–K plots and CIA estimates of PRB forearc sediments and bedrocks (a) and schematic diagram (b) showing theoretical compositional change during chemical weathering and/or physical sorting. Oxides are expressed in molar fractions. All compositions are normalized to 100% on a volatile-free basis. For the San Diego forearc samples, carbonate corrected compositions are also included. (For interpretation of the colors in the figure(s), the reader is referred to the web version of this article.)

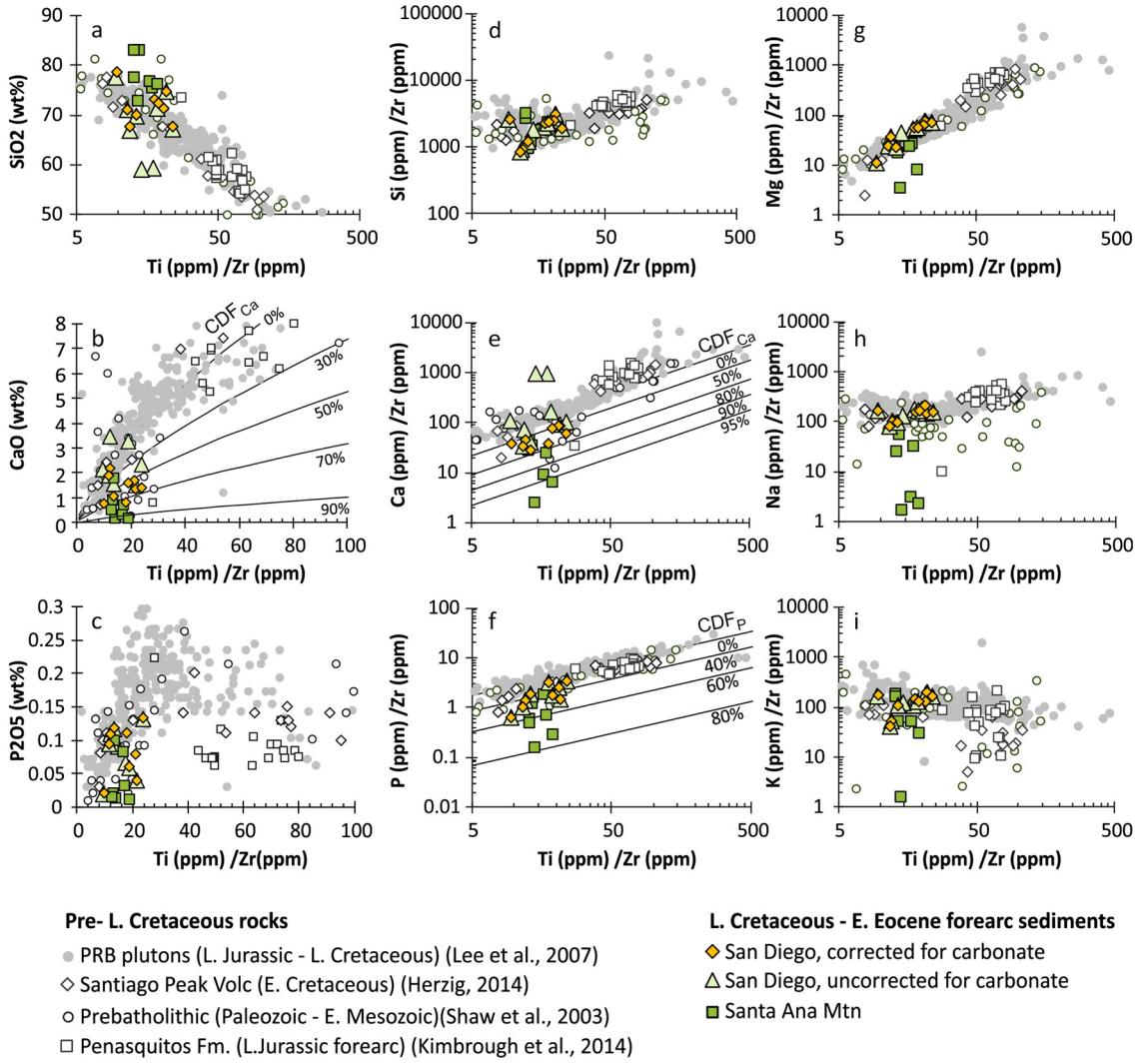

Fig. 6. Comparison between the bulk rock composition of the Upper Cretaceous–Lower Eocene forearc sediments (this study) and compositions of PRB plutonic rocks. All the compositions are normalized to 100% on a volatile free basis. Bulk rock composition of the prebatholithic metasediments (Shaw et al., 2003), Santiago Peak Volcanics (Herzig and Kimbrogh, 2014) and sediments from the Late Jurassic forearc (Kimbrough et al., 2014) are also included. Thin curves in Fig. 6b, e, and f are modeled compositions of the sediments assuming the parent rocks are PRB plutonic rocks with various degrees of chemical depletion. Symbols are the same with Fig. 5.

In Fig. 5a, PRB sediment bulk compositions plot above the plutonic rock trend, suggesting moderate to intense chemical weathering. In particular, samples from the Santa Ana Mountains display a chemical weathering trend, suggesting that the deviation of the sediment composition from plutonic rock composition is primarily caused by chemical weathering. Physical sorting appears to play a minor control, which is consistent with the Th/Sc vs Zr/Sc systematics (Fig. 4).

5.2. Elemental depletion fraction and weathering fluxes

In Fig. 6 we further evaluate chemical depletion of mobile elements in the forearc sediments by plotting mobile/immobile elemental ratios versus Ti/Zr (ppm/ppm). Magmatic differentiation, as recorded in the bulk plutonic rock compositions, exhibit negative correlations between Si/Zr versus Ti/Zr and positive correlations between Mg/Zr, Ca/Zr and P/Zr versus Ti/Zr (Fig. 6a–g). Na/Zr shows only minor variation with Ti/Zr, and K/Zr shows a negative correlation with Ti/Zr (Fig. 6h–i).

In general, Ti/Zr ratios in the sediments range between 2 to 25, suggesting that the parent rocks have SiO_2 > 55% and thus have felsic protoliths (Fig. 6a). Si shows slight enrichment in the sediment, likely due to concentration of quartz or development of silica cement. However, on the Ca/Zr, Na/Zr, Mg/Zr and P/Zr vs Ti/Zr diagrams, we see that many fall below the plutonic trend, suggesting depletion of these elements. The most pronounced depletions are seen in Ca and P (Fig. 6b, c, e, f). Using an empirical fit between Ca/Zr and Ti/Zr for plutonic rocks, $\log_{10}(\mathrm{Ca/Zr}) = 1.065 * \log_{10}(\mathrm{Ti/Zr}) + 0.857 \pm 0.158(1\sigma)$ ($R^2 = 0.85$), we estimate total depletion fractions of Ca ($\mathrm{CDF_{Ca}}$) to be 0.4–0.8 from the San Diego samples and 0.6–1 from the Santa Ana Mountain samples. For the San Diego samples, which have variable amounts of carbonate, we plot compositions with and without correction for carbonate content. We note that even without correction, four samples still plot below the plutonic array, suggesting that Ca loss in the San Diego samples is not a result of over-correction for carbonate content.

Since trace amount of apatite and calcite are universally present in granitoids, of side interest here is how much of the Ca loss might be attributed to dissolution of accessory apatite and calcite. For apatite, using a P/Zr vs Ti/Zr diagram (Fig. 6f), we show that there is ~40% P depletion in the forearc sediments. The average CaO and P_2O_5 concentration in PRB plutonic rocks with Ti/Zr between 5–50 is 4 ± 1.6 wt% and 0.17 ± 0.06 wt%, respectively (Lee et al., 2007). Since P is primarily hosted in apatite, apatite dissolution contributes ~5% to the total Ca loss from weathering. For igneous calcite, there is no known measurements in the PRB plu-

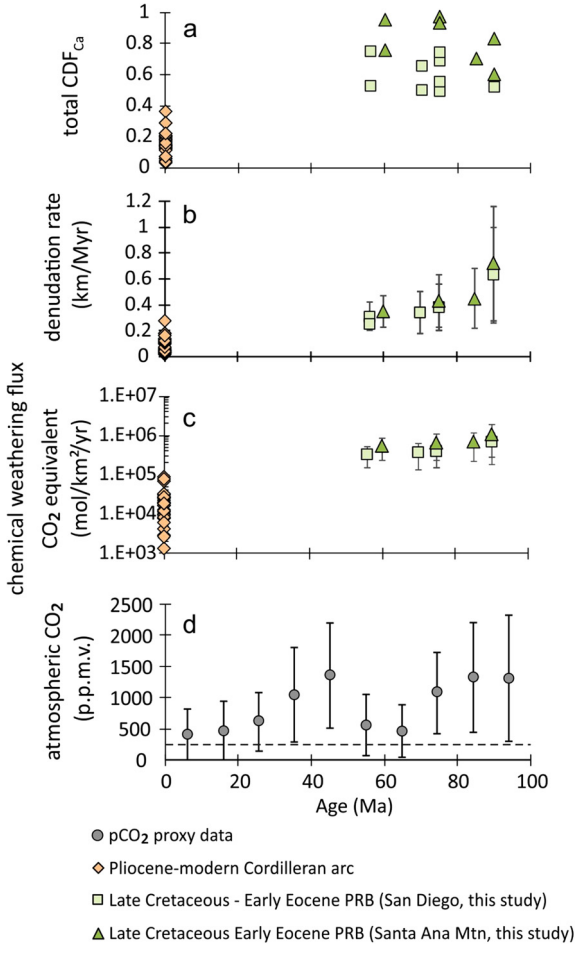

Fig. 7. Variations in the chemical depletion fraction (CDF) of Ca, denudation rate and weathering flux (in CO_2 equivalent) in the Cordilleran arc compared to Pliocene-modern quantities in similar bedrock, and variations in atmospheric pCO_2 since the Late Cretaceous. The Pliocene-modern chemical weathering flux (Fig. 7c) were determined from soil and regolith profile measurements from Riebe et al. (2004) (Sierra Nevada), Dixon et al. (2012) (Transverse Ranges), and Girty et al. (2014) (PRB), as well as river solute flux from West et al. (2005) (Sierra Nevada). Atmospheric pCO_2 proxy data are taken from a variety of paleo-CO_2 compilations by Krissansen-Totton and Catling (2017). Dashed line represents the average Pleistocene pCO_2 level as a reference line.

tonic rocks, but study by White et al. (2005) suggests an average concentration of 2.52 g/kg calcite in granitoids. Therefore, dissolution of accessory calcite from igneous rocks, if primary, contributes to at most ~3% of the total Ca loss from weathering.

For other chemical weathering related base cations, we only observed moderate to strong depletion in Na in some of the samples from Santa Ana Mountains. We did not observe distinct Mg and K depletion except in two Santa Ana Mountains samples (Fig. 6g–i). Moderate to slight depletion of Mg, K and Na may be a result of retention of these elements in clay minerals in the weathering products (Sawhney, 1972; Babechuk et al., 2014). However, we also note that the low concentrations of these elements in both batholithic and sedimentary rocks, combined with scatter in the "plutonic array", makes it difficult to determine depletion fraction for these elements. In the following section, we use our carbonate-corrected Ca flux to approximate the minimum CO_2 drawdown flux. We estimated the weathering flux from the PRB during the Late Cretaceous–Early Eocene using the denudation rates from Jiang and Lee (2017) (0.1–1 km/Myr) (supplementary Table 1), the average CaO from PRB plutonic rocks with Ti/Zr of 5–50 (4%), and the average CDF_{Ca} from weathering inferred from the forearc sediment geochemistry (60% in San Diego samples and 85% in Santa Ana Mountains samples) using Eq. (5). The Ca weathering fluxes or CO_2 consumption rates in the PRB from the Late Cretaceous to Early Eocene are estimated to be (2–10) $\times 10^5$ mol/km^2/yr (Figs. 6c, 7a). Uncertainty in the weathering flux is estimated to be 40–70% (1σ) from the combined uncertainties in the total denudation rate (30%), the CDF_{Ca} (20%) and inferred CaO concentration (40%) in the PRB protolith.

5.3. Additional complications

The assumption we made in calculating the chemical weathering flux (in equivalent CO_2) in the PRB is that the chemical difference between the forearc sediments and PRB rocks is mainly a result of elemental loss/gain during erosion of fresh batholithic rocks. However, complications in source rock composition, sedimentary and diagenetic processes may contribute to the calculated chemical depletion fractions. For example, a small fraction of the sediments in the Santa Ana Mountain samples were derived from high-silica metamorphic rocks, such as quartzite, which have low concentrations of Ca and other base cations and may result in overestimation of the bulk CDF_{Ca}. Sedimentary processes can also introduce variability in the apparent chemical depletion fraction (Lupker et al., 2012). However, as we showed earlier in this section and Fig. 4, physical sorting played a minor role in modifying the bulk compositions in the forearc sediments. Given that the forearc sediments are proximal deposits in a tectonically active region and that they have only recently been exposed to the surface, we believe that bulk compositions in the forearc sediments capture the primary chemical weathering signature of the Late Cretaceous–Early Eocene. Uncertainties in the total denudation rate and parent rock composition are the major sources of uncertainty in estimating the weathering flux.

6. Discussion

6.1. Long term carbon balance/imbalance in continental arc

Modern weathering rates have been estimated to be (0.01–3) $\times 10^5$ mol/km^2/yr (equivalent CO_2) based on soil profiles in felsic terranes and ~0.6 $\times$ 10^5 mol/km^2/yr based on Ca + Mg cation fluxes from large rivers (Gaillardet et al., 1999; Riebe et al., 2004; West et al., 2005). Both estimates are lower than that inferred for the Cretaceous–Paleogene PRB setting investigated here. A compilation of CDF_{Ca}, total denudation rate and weathering rates (equivalent CO_2) in the Late Cretaceous–Early Eocene PRB and its modern counterparts in the Cordilleran arc (Fig. 7) shows that erosion dominates the weathering rate in this arc segment since the Late Cretaceous. Higher pCO_2 conditions during the Late Cretaceous–Early Eocene may favor higher silicate weathering reaction kinetics, resulting in higher weathering intensity, as reflected in CDF_{Ca} values. Our results suggest that arc orogens can contribute significant weathering flux, largely because of the enhanced erosion associated with active arc orogens. Given that the magmatic orogens also produce CO_2 through magmatism and metamorphism, the question then is whether magmatic orogens serve as a net carbon source or sink over the course of its lifetime. Below, we estimate CO_2 production from the PRB and compare it to the regional CO_2 consumption rates calculated in section 5.

To estimate CO_2 production, we adopt the approach by Marty and Tolstikhin (1998). Here, CO_2 flux ($J_{C,arc}$, mol/km^2/yr) from subduction zones is calculated as:

$$J_{C,arc} = \dot{M}_{arc} \cdot \rho_{magma} \cdot \left[^3\mathrm{He}\right]_{um} \cdot \left(C/^3\mathrm{He}\right)_{arc} \cdot r_{arc}^{-1} \quad (8)$$

where $\dot{M}_{arc}$ is the volumetric flux of arc magmas (km^3/km^2/Myr), ρ_{magma} is the density of magma (2500 kg/m^3), r_{arc} is the degree

of partial melting at arcs, $[^3He]_{um}$ is the concentration of ^3He of depleted upper mantle (mol/g), $(C/^3He)_{arc}$ is the $C/^3He$ ratio of gas from the volcano type of interest. Helium is used for two reasons. First, the absolute concentration of carbon in volcanic gases, let alone the volcanic flux of C, is very difficult to quantify. Second, the ^3He flux can be reasonably well calculated. ^3He in volcanic gases is thought to come only from the mantle and therefore the magmatic flux of ^3He can be forward modeled if the ^3He concentration of the mantle and the average melting degree is known. The C flux can then be estimated by multiplying the ^3He flux by the characteristic $C/^3He$ ratio, a quantity that can be measured.

Magmatic addition rate in the PRB between 130 and 80 Ma is 0.1–2 km/My (Jiang and Lee, 2017). We assume a melting degree for primary parental magmas of the PRB to be ~0.1 based on incompatible elements, such as K concentration in PRB plutonic rocks (Lee et al., 2007). $[^3He]_{um}$ was assumed to be $(2.5 \pm 1.5) \times 10^{-15}$ mol/g following Tolstihkhin and Marty (1998). There is no direct way of estimating the $CO_2/^3He$ ratio of PRB volcanism during the Cretaceous. However, we can take modern continental arcs as possibly being representative. The present-day global average $CO_2/^3He$ from continental arc volcanic gases is $(20 \pm 3) \times 10^9$ (Sano and Williams, 1996; Mason et al., 2017). Using these quantities in Eq. (8), we estimate magmatic CO_2 fluxes in the Late Cretaceous PRB in Fig. 8a.

These magmatic fluxes are compared to the CO_2 consumption fluxes estimated from our observed weathering rates. Since the sedimentary record for the Early Cretaceous (during the magmatic flare-up) is missing in our study areas, for completeness, we estimate CO_2 consumption rates during this time using on a simple model of erosion (Jiang and Lee, 2017) and adopting an average CaO concentration in the PRB rocks (4%) and average CDF_{Ca} (60%) for forearc samples (green band in Fig. 8a). Denudation rates were modeled assuming magmatic addition drives crustal thickening, surface uplift and erosion, with a 4 Ma erosion response time (details in Jiang and Lee, 2017).

Despite large uncertainties, it can be seen that the time-integrated CO_2 production and consumption fluxes in the PRB, from the beginning of magmatism to after magmatism ends, are of the same order of magnitude, 10^5–10^6 mol/km^2/yr. In detail, however, the PRB was a regional carbon source during the Late Cretaceous magmatic flare-up, but after magmatism ended, remnant topography allowed erosion to continue. As a result, the arc transitioned from a net regional carbon source in the Cretaceous to a net regional carbon sink in the Early Eocene (Fig. 8b). Thus, although the total time-integrated amount of CO_2 released from the arc appears to be balanced by CO_2 consumption through silicate weathering of arc rocks, production and consumption were not in phase.

We note that both arc CO_2 production and consumption rates estimated here are likely lower bounds. For CO_2 consumption, including the maximum modeled denudation rates from Jiang and Lee (2017) as well as the weathering flux of Mg, could increase our regional CO_2 consumption rates by at most two to three times. For CO_2 production, the magmatic addition rate and the $CO_2/^3He$ ratio in volcanic gases are uncertain for ancient systems (Wallace, 2005; Lee and Lackey, 2015; Jiang and Lee, 2017; Mason et al., 2017). In particular, if the amount of CO_2 degassing via carbonate-magma interaction is much larger than that represented by modern continental arc volcanism, the time-integrated CO_2 production in the PRB could exceed CO_2 consumption through silicate weathering in the arc (Lee et al., 2013; Lee and Lackey, 2015; Carter and Dasgupta, 2016; Carter and Dasgupta, 2018). On a global scale, this extra CO_2 input through magmatism must be balanced by other outputs of CO_2 away from the arc itself, that is, through seafloor weathering or enhanced weathering in continental interiors (Kent and Muttoni, 2013; Mills et al., 2014; Jagoutz et al., 2016).

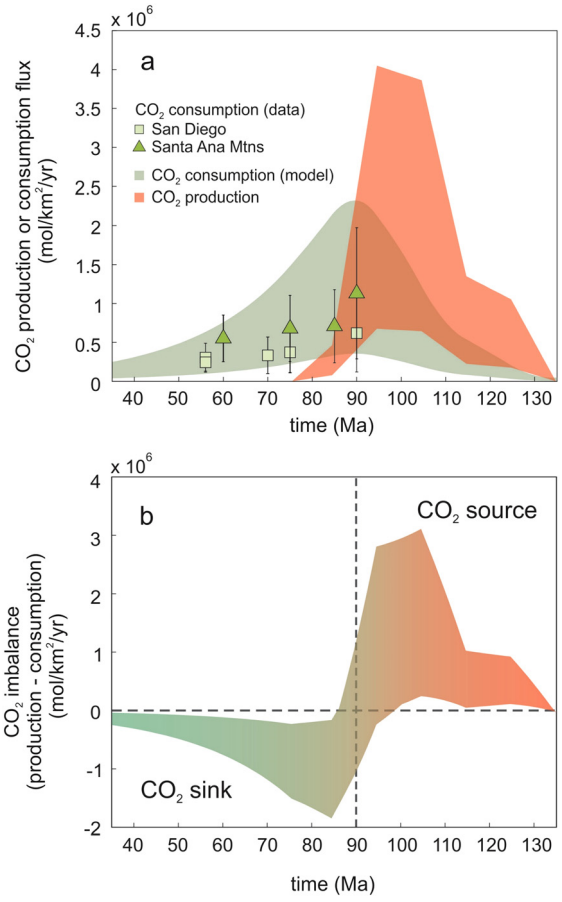

Fig. 8. a) Variation in CO_2 production and consumption with time in the PRB. Symbols with error bar are consumption fluxes calculated based on the bulk rock geochemistry in the forearc sediments from this study and erosion rates derived from detrital geochronology and thermobarometry in Jiang and Lee (2017). Error bars in the CO_2 consumption flux are 1σ. Green curve represents the consumption fluxes calculated using the average observed CDF_{Ca} in forearc sediments and erosion rates from a coupled magmatism – erosion model in Jiang and Lee (2017). Red curve represents the CO_2 production fluxes calculated using magmatic addition rates from Jiang and Lee (2017) and average CO_2 concentration in continental arc magmas. b) Net CO_2 fluxes in the arc, calculated from subtraction of the production curve by the consumption curve in Fig. 8a. The arc was a net CO_2 source during magmatic flare-up, but became a net CO_2 sink after cessation of magmatism.

6.2. *Effect of continental arcs on silicate weathering feedback strength*

Variation in both weathering rate and extent of weathering in Cordilleran arc segments since the Late Cretaceous reflects an interplay between tectonic uplift and climate over the evolution of a continental arc orogen (Fig. 7). High relief regions have been considered to represent regions with both high "erodibility" and sensitive response to climate change due to fast erosion and high water runoff (orogenic precipitation), thus the distribution of mountainous regions may have a profound influence on the global weathering – climate feedback strength, which regulates long term atmospheric pCO_2 (Riebe et al., 2004; West et al., 2005; Hilley et al., 2010; Maher and Chamberlain, 2014; Caves Rugenstein et al., 2019). Given that continental arc development is a mountain building process (Lee et al., 2015; Jiang and Lee, 2017), variation in the global continental arc length over geologic history (Cao et al., 2017) might have contributed to both global CO_2 production and the negative climate feedback strength.

To illustrate the contribution of magmatic orogens to the long-term climate feedback, we consider a simplified model, which assumes that continents consists of two parts: a mountainous region and a flat continental interior. The global silicate weathering rate (mol/yr or tons/yr) is the sum of silicate weathering from low relief continental interiors F_{ci} and from mountainous regions F_m:

$$F_{silw} = F_m + F_{ci} \tag{9}$$

Assuming constant total continental area, the relative global silicate weathering rate at time t when normalized to that of today can be expressed as:

$$R_{Fsil} = \frac{F^t_{silw}}{F^0_{silw}} = \frac{\alpha_0}{\alpha_t} \cdot \frac{(1 - f^t_m) \cdot \alpha_t + f^t_m}{(1 - f^0_m) \cdot \alpha_0 + f^0_m} \tag{10}$$

where f_m is the areal fraction of mountains in the continents, and α is the ratio between chemical weathering rates in continental interiors to that in mountainous areas:

$$\alpha = \frac{D_{ci} \cdot f_{sil} \cdot CDF_{ci}}{D_m \cdot f_{sil} \cdot CDF_m} \tag{11}$$

where D_m and D_{ci} are the denudation rates (tons/km^2/yr) in mountains and continental interiors, respectively, f_{sil} is the weight fraction of cations that directly related to silicate weathering (Ca + Mg + Na + K) in upper continental crust rocks (~8% by cation weight) (Rudnick and Fountain, 1995; West et al., 2005), and *CDF* is the chemical depletion fraction of these silicate cations (e.g., weathering intensity). Assuming mountainous regions and continental interiors have a characteristic denudation rate, the ratio between present day α to that at time t represents weathering intensity CDF_m normalized to the present day, which scales to relative climate feedback strength:

$$\frac{\alpha_0}{\alpha_t} = \frac{CDF^t_m}{CDF^0_m} = R_{CDF_m} \tag{12}$$

Continental interiors are typified by supply-limited chemical weathering, in which weathering reaction rates exceed the conversion rate of bedrock to soil (West et al., 2005), hence we assume for simplicity that CDF_{ci} approaches 100%. However, denudation rates in continental interiors are too low to contribute significantly to global weathering flux, even with high weathering intensity (Hartmann et al., 2009). In contrast, mountainous regions is typified by high denudation rates and kinetically limited weathering due to short soil residence time, thus CDF_m varies with changes in global and regional climate (Riebe et al., 2004; West et al., 2005). Eq. (10) suggests that if continental area and composition do not change significantly, variation in global silicate weathering flux at any given time is primarily controlled by changes in the areal fraction and weathering intensity in mountainous regions. Assuming $\alpha_0 = 0.1$ (West et al., 2005; Maher and Chamberlain, 2014) and $f^0_m = 0.1$ (Tanner, 1962), in Fig. 9a we calculated the variation in global silicate weathering rate R_{Fsil} with areal fraction of mountains for different R_{CDF_m}. The Late Cretaceous is characterized by continental arc length twice that of today, resulting in 2–10 times higher pCO_2 level and doubled R_{CDF_m} compared with that today (Park and Royer, 2011; Cao et al., 2017) (Fig. 7), suggesting a stronger climate-silicate weathering feedback during the Late Cretaceous.

Using the relation between reaction kinetics, temperature and pCO_2 (Brady, 1991; West et al., 2005), R_{CDF_m} can be roughly scaled to pCO_2. Fig. 9b shows a semi-quantitative relation between global CO_2 uptake rate and stabilized pCO_2 under different areal fractions of mountainous regions, such as continental arcs. Since the CO_2 production and consumption are balanced on >My timescales, this CO_2 uptake rate also equals the CO_2 production rate. In Fig. 9b, point 1 represents present day conditions. Enhanced continental arc activities through magmatic flare-ups during the Late Cretaceous results in increased CO_2 production, as well as stronger feedback due to the high erosion rates accompanying the development of an arc orogen (point 1 to 2). With decreased activity in arc magmatism, CO_2 production decreases, and the topographical remnants of continental arcs continue to erode. Eventually, global feedback strength returns to the original level (point 2 to 1) when erosion causes topography to disappear.

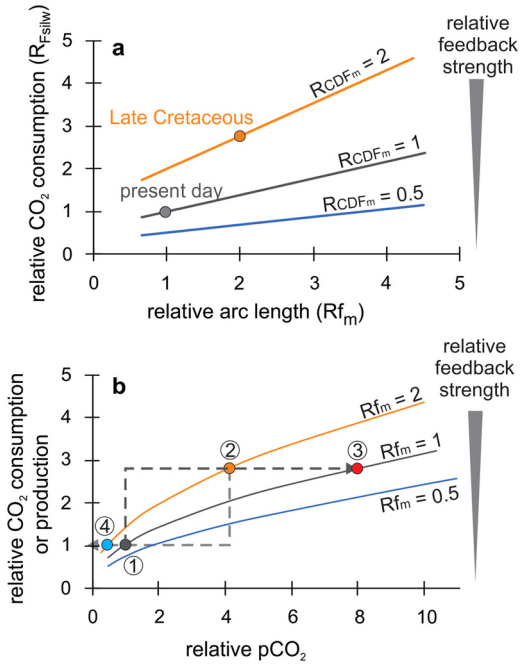

Fig. 9. a) Relative CO_2 consumption varies with relative length of continental arcs (mountainous area) (normalized to present day values). Different curves were constructed assuming different sensitivity of chemical weathering in mountains to climate (R_{CDF_m}). Present day and approximate Late Cretaceous values are plotted on both diagrams for reference. b) Semi-quantitative diagram showing different stabilized pCO_2 levels depending on CO_2 production and the climate – silicate weathering feedback strength. Increase in mountainous areas result in increase in the feedback strength. Point 1–4 represents conditions following different hypothetical tectonic evolution paths (dashed lines) (details see text in section 6.2).

This variation in feedback strength associated with continental arc development thus serves as a "buffer" to prevent the system from veering into extreme climate. For example, although continental arcs contribute considerable amounts of CO_2 production, with enhanced climate feedback due to the arc orogen development, pCO_2 can be stabilized at a lower level compared to a system without changes in the feedback strength (point 2 vs 3). Similar control of feedback strength in stabilizing pCO_2 can be predicted when the system experiences a decrease in CO_2 production (point 1 vs 4). It also follows that in order to maintain high pCO_2 in the Cretaceous when global silicate weathering efficiency was likely higher, even higher volcanic or metamorphic degassing of CO_2 is required. Finally, weathering of these remnant orogens after magmatism terminates would drive the system towards cooler climates. Caves Rugenstein et al. (2019) showed that Cenozoic cooling was associated with decreased weathering intensity but increased global erosion. Our study suggests that erosion of magmatically dead Cretaceous orogenic belts, not just the Himalayas, may contribute to the global erosion rate (Lee et al., 2015).

7. Conclusions

In this study, we introduced a method to constrain long term chemical weathering flux in continental arcs by comparing the geochemistry of fore-arc sediments to that of parent batholithic rocks. We show that the Late Cretaceous–Early Eocene Peninsular Ranges continental arc in California, USA was characterized by high chemical weathering flux due to high denudation rates in the arc. Our minimum estimates on both CO_2 production and consumption rates in the PRB suggests that total CO_2 consumption integrated over the topographic lifetime of the orogen was comparable to the CO_2 production through the arc. However, CO_2 production and consumption are out of phase, in the way that during magmatism, CO_2 degassing exceeds the regional weathering output, whereas during the decline of magmatism and after magmatism, regional weathering rates exceed CO_2 degassing. Because magmatism and erosion are coupled in the continental magmatic arcs, arcs can serve as either a net source or sink of carbon depending on the stage of arc development. We note that given the uncertainties in magmatic addition rate and crustal composition, the time-integrated CO_2 production in the PRB could be much higher. Globally, this extra CO_2 input must be balanced by other outputs of CO_2 away from the arc.

As mountain building processes are often accompanied with development of continental arcs, we propose that enhanced continental arc activities will increase global inputs of CO_2 during the flare-up stage, but at the same time, the development of arcs increases global weatherability, resulting in a strengthened global negative feedback between silicate weathering and climate. Therefore, variations in continental arc length in geologic history due to tectonic reconfiguration may play an important role in modulating atmospheric pCO_2.

Acknowledgements

This study was supported by an NSF grant to understand the role of continental arcs in long term climate evolution to Lee (OCE-1338842) and a Geological Society of America Grant to Jiang. We thank Lexi Malouta for assistance in sample collection, and Dr. Scott Boroughs from the Peter Hooper Geoanalytical Lab for the XRF analyses. We also appreciate Mark Torres, Rajdeep Dasgupta and Laurence Yeung for discussions on the long-term carbon cycle. We thank an anonymous reviewer for constructive reviews.

Appendix A. Supplementary material

Supplementary material related to this article can be found online at https://doi.org/10.1016/j.epsl.2019.115733.

References

Babechuk, M.G., Widdowson, M., Kamber, B.S., 2014. Quantifying chemical weathering intensity and trace element release from two contrasting basalt profiles, Deccan Traps, India. Chem. Geol. 363, 56–75.

Bahlburg, H., Dobrzinski, N., 2011. Chapter 6 A review of the Chemical Index of Alteration (CIA) and its application to the study of Neoproterozoic glacial deposits and climate transitions. Mem. Geol. Soc. Lond. 36 (1), 81.

Berner, R.A., 1991. A model for atmospheric CO_2 over Phanerozoic time. Am. J. Sci. 291 (4), 339–376.

Berner, R.A., 1994. GEOCARB II; a revised model of atmospheric CO_2 over Phanerozoic time. Am. J. Sci. 294 (1), 56–91.

Berner, R.A., Caldeira, K., 1997. The need for mass balance and feedback in the geochemical carbon cycle. Geology 25 (10), 955–956.

Berner, R.A., Lasaga, A.C., Garrels, R.M., 1983. The carbonate-silicate geochemical cycle and its effect on atmospheric carbon dioxide over the past 100 million years. Am. J. Sci. 283 (7), 641–683.

Brady, P.V., 1991. The effect of silicate weathering on global temperature and atmospheric CO_2. J. Geophys. Res., Solid Earth 96 (B11), 18101–18106.

Brimhall, G.H., Dietrich, W.E., 1987. Constitutive mass balance relations between chemical composition, volume, density, porosity, and strain in metasomatic hydrochemical systems: results on weathering and pedogenesis. Geochim. Cosmochim. Acta 51 (3), 567–587.

Cao, W., Lee, C.-T.A., Lackey, J.S., 2017. Episodic nature of continental arc activity since 750 Ma: a global compilation. Earth Planet. Sci. Lett. 461, 85–95.

Carter, L.B., Dasgupta, R., 2016. Effect of melt composition on crustal carbonate assimilation: implications for the transition from calcite consumption to skarnification and associated CO_2 degassing. Geochem. Geophys. Geosyst. 17 (10), 3893–3916.

Carter, L.B., Dasgupta, R., 2018. Decarbonation in the Ca-Mg-Fe carbonate system at mid-crustal pressure as a function of temperature and assimilation with arc magmas – implications for long-term climate. Chem. Geol. 492, 30–48.

Caves, J.K., Jost, A.B., Lau, K.V., Maher, K., 2016. Cenozoic carbon cycle imbalances and a variable weathering feedback. Earth Planet. Sci. Lett. 450, 152–163.

Caves Rugenstein, J.K., Ibarra, D.E., von Blanckenburg, F., 2019. Neogene cooling driven by land surface reactivity rather than increased weathering fluxes. Nature 571 (7763), 99–102.

Dixon, J.L., Hartshorn, A.S., Heimsath, A.M., DiBiase, R.A., Whipple, K.X., 2012. Chemical weathering response to tectonic forcing: a soils perspective from the San Gabriel Mountains, California. Earth Planet. Sci. Lett. 323–324, 40–49.

Gaillardet, J., Dupré, B., Louvat, P., Allègre, C.J., 1999. Global silicate weathering and CO_2 consumption rates deduced from the chemistry of large rivers. Chem. Geol. 159 (1–4), 3–30.

Girty, G.H., 1987. Sandstone provenance, Point Loma Formation, San Diego, California: evidence for uplift of the Peninsular Ranges during the Laramide Orogeny. J. Sediment. Petrol. 57 (5), 839–844.

Girty, G.H., et al., 2014. Reconstructing the regolith from erosionally exhumed corestone and saprock derived from the Cretaceous Val Verde tonalite, Peninsular Ranges, southern California, USA: a case study. Catena 113, 150–164.

Grove, M., Lovera, O., Harrison, M., 2003. Late Cretaceous cooling of the east-central Peninsular Ranges batholith (33°N): relationship to La Posta pluton emplacement, Laramide shallow subduction, and forearc sedimentation. In: Johnson, S.E., et al. (Eds.), Tectonic Evolution of Nortwestern Mexico and the Southwestern USA. In: Geological Society of America Special Paper, vol. 374. GSA, Boulder, Colorado, pp. 355–397.

Hartmann, J., Jansen, N., Dürr, H.H., Kempe, S., Köhler, P., 2009. Global CO_2-consumption by chemical weathering: what is the contribution of highly active weathering regions? Glob. Planet. Change 69 (4), 185–194.

Herzig, C.T., Kimbrogh, D.L., 2014. Santiago Peak volcanics: early Cretaceous arc volcanism of the western Peninsular Ranges Batholith, southern California. In: Morton, D.M., Miller, F.K. (Eds.), Peninsular Ranges Batholith, Baja California and Sourthern California. Geological Society of America Memoir, vol. 211, pp. 345–363.

Hilley, G.E., Chamberlain, C.P., Moon, S., Porder, S., Willett, S.D., 2010. Competition between erosion and reaction kinetics in controlling silicate-weathering rates. Earth Planet. Sci. Lett. 293 (1), 191–199.

Holland, H.D., 1984. The Chemical Evolution of the Atmosphere and Oceans. Princeton University Press, Princeton, NJ.

Jagoutz, O., Macdonald, F.A., Royden, L., 2016. Low-latitude arc–continent collision as a driver for global cooling. Proc. Natl. Acad. Sci. USA 113 (18), 4935.

Jiang, H., Lee, C.-T.A., 2017. Coupled magmatism–erosion in continental arcs: reconstructing the history of the Cretaceous Peninsular Ranges batholith, southern California through detrital hornblende barometry in forearc sediments. Earth Planet. Sci. Lett. 472, 69–81.

Johnson, D.M., Hooper, P.R., Conrey, R.M., 1999. XRF analysis of rocks and minerals for major and trace elements on a single low dilution Li-tetraborate fused bead. Adv. X-Ray Anal. 41, 843–867.

Kent, D.V., Muttoni, G., 2013. Modulation of Late Cretaceous and Cenozoic climate by variable drawdown of atmospheric pCO_2 from weathering of basaltic provinces on continents drifting through the equatorial humid belt. Clim. Past 9 (2), 525–546.

Kimbrough, D.L., et al., 2001. Forearc-basin sedimentary response to rapid Late Cretaceous batholith emplacement in the Peninsular Ranges of southern and Baja California. Geology 29 (6), 491–494.

Kimbrough, D.L., et al., 2014. Upper Jurassic Peñasquitos Formation—forearc basin western wall rock of the Peninsular Ranges batholith. In: Geological Society of America Memoirs, vol. 211, pp. 625–643.

Krissansen-Totton, J., Catling, D.C., 2017. Constraining climate sensitivity and continental versus seafloor weathering using an inverse geological carbon cycle model. Nat. Commun. 8, 15423.

Kump, L.R., Arthur, M.A., 1999. Interpreting carbon-isotope excursions: carbonates and organic matter. Chem. Geol. 161 (1), 181–198.

Lee, C.-T.A., Bachmann, O., 2014. How important is the role of crystal fractionation in making intermediate magmas? Insights from Zr and P systematics. Earth Planet. Sci. Lett. 393, 266–274.

Lee, C.-T.A., Morton, D.M., Kistler, R.W., Baird, A.K., 2007. Petrology and tectonics of Phanerozoic continent formation: from island arcs to accretion and continental arc magmatism. Earth Planet. Sci. Lett. 263, 370–387.

Lee, C.-T.A., et al., 2013. Continental arc-island arc fluctuations, growth of crustal carbonates, and long-term climate change. Geosphere 9 (1), 1–16.

Lee, C.-T.A., Thurner, S., Paterson, S.R., Cao, W., 2015. The rise and fall of continental arcs: interplays between magmatism, uplift, weathering, and climate. Earth Planet. Sci. Lett. 425, 105–119.
Lee, C.T.A., Lackey, J.S., 2015. Global continental arc flare-ups and their relation to long-term greenhouse conditions. Elements 11, 125–130.
Lupker, M., et al., 2012. Predominant floodplain over mountain weathering of Himalayan sediments (Ganga basin). Geochim. Cosmochim. Acta 84, 410–432.
Maher, K., Chamberlain, C.P., 2014. Hydrologic regulation of chemical weathering and the geologic carbon cycle. Science 343 (6178), 1502.
Manger, G.E., 1963. Porosity and bulk density of sedimentary rocks. USGS Surv. Bull. 1144E.
Marty, B., Tolstikhin, I.N., 1998. CO_2 fluxes from mid-ocean ridges, arcs and plumes. Chem. Geol. 145 (3–4), 233–248.
Mason, E., Edmonds, M., Turchyn, A.V., 2017. Remobilization of crustal carbon may dominate volcanic arc emissions. Science 357 (6348), 290.
Mckenzie, N.R., Hughes, N.C., Gill, B.C., Myrow, P.M., 2014. Plate tectonic influences on Neoproterozoic-early Paleozoic climate and animal evolution. Geology 42 (2), 127–130.
Middelburg, J.J., van der Weijden, C.H., Woittiez, J.R.W., 1988. Chemical processes affecting the mobility of major, minor and trace elements during weathering of granitic rocks. Chem. Geol. 68 (3), 253–273.
Mills, B., Daines, S.J., Lenton, T.M., 2014. Changing tectonic controls on the long-term carbon cycle from Mesozoic to present. Geochem. Geophys. Geosyst. 15 (12), 4866–4884.
Morton, D.M., et al., 2014. Framework and petrogenesis of the northern Peninsular Ranges batholith, southern California. Mem. Geol. Soc. Amer. 211, 61–143.
Nesbitt, H.W., 1979. Mobility and fractionation of rare earth elements during weathering of a granodiorite. Nature 279 (5710), 206–210.
Nesbitt, H.W., Young, G.M., 1984. Prediction of some weathering trends of plutonic and volcanic rocks based on thermodynamic and kinetic considerations. Geochim. Cosmochim. Acta 48 (7), 1523–1534.
Nesbitt, H.W., Young, G.M., McLennan, S.M., Keays, R.R., 1996. Effects of chemical weathering and sorting on the petrogenesis of siliciclastic sediments, with implications for provenance studies. J. Geol. 104 (5), 525–542.
Park, J., Royer, D.L., 2011. Geologic constraints on the glacial amplification of Phanerozoic climate sensitivity. Am. J. Sci. 311 (1), 1–26.
Premo, W.R., Morton, D.M., Wooden, J.L., Fanning, C.M., 2014. U–Pb zircon geochronology of plutonism in the northern Peninsular Ranges batholith, southern California: implications for the Late Cretaceous tectonic evolution of southern California. In: Morton, D.M., Miller, F.K. (Eds.), Peninsular Ranges Batholith, Baja California and Southern California. In: Geological Society of America Memoir, vol. 211, pp. 145–180.
Riebe, C.S., Kirchner, J.W., Finkel, R.C., 2003. Long-term rates of chemical weathering and physical erosion from cosmogenic nuclides and geochemical mass balance. Geochim. Cosmochim. Acta 67 (22), 4411–4427.
Riebe, C.S., Kirchner, J.W., Finkel, R.C., 2004. Erosional and climatic effects on long-term chemical weathering rates in granitic landscapes spanning diverse climate regimes. Earth Planet. Sci. Lett. 224 (3–4), 547–562.
Rudnick, R.L., Fountain, D.M., 1995. Nature and composition of the continental crust: a lower crustal perspective. Rev. Geophys. 33 (3), 267–309.
Sano, Y., Williams, S.N., 1996. Fluxes of mantle and subducted carbon along convergent plate boundaries. Geophys. Res. Lett. 23 (20), 2749–2752.
Sawhney, B.L., 1972. Selective sorption and fixation of cations by clay minerals: a review. Clays Clay Miner. 20, 93–100.
Schoellhamer, J.E., Vedder, J.G., Yerkes, R.F., Kinney, D.M., 1981. Geology of the Northern Santa Ana Mountains, California. U.S. Geological Survey Professional Paper 420-D. 109 pp.
Sharman, G.R., Graham, S.A., Grove, M., Kimbrogh, D.L., Wright, J.E., 2015. Detrital zircon provenance of the Late Cretaceous-Eocene California forearc: influence of Laramide low-angle subduction on sediment dispersal and paleogeography. Geol. Soc. Am. Bull. 127 (1-2), 38–60.
Shaw, H.R., Todd, V.R., Grove, M., 2003. Jurassic peraluminous gneissic granites in the axial zone of the Peninsular Ranges, southern California. In: Johnson, S.E., et al. (Eds.), Tectonic Evolution of Northwestern Mexico and the Southwestern USA. In: Geological Society of America Special Paper, vol. 374, pp. 157–183.
Sundquist, E.T., 1991. Steady- and non-steady-state carbonate-silicate controls on atmospheric CO_2. Quat. Sci. Rev. 10, 283–296.
Tanner, W.F., 1962. Components of the hypsometric curve of the Earth. J. Geophys. Res. 67 (7), 2841–2843.
Taylor, S.R., McClennan, S.M., 1985. The Continental Crust: Its Composition and Evolution. Blackwell, Oxford.
Thomson, C.N., Girty, G.H., 1994. Early Cretaceous intra-arc ductile strain in Triassic-Jurassic and Cretaceous continental margin arc rocks, Peninsular Ranges, California. Tectonics 13 (5), 1108–1119.
Todd, V.R., Erskine, B.G., Morton, D.M., 1988. Metamorphic and tectonic evolution of the northern Peninsular Ranges Batholith, southern California. In: Ernst, W.G. (Ed.), Metamorphism and Crustal Evolution of the Western United States (Rubey Volume 7), pp. 894–937.
Tolstikhin, I.N., Marty, B., 1998. The evolution of terrestrial volatiles: a view from helium, neon, argon and nitrogen isotope modelling. Chem. Geol. 147 (1–2), 27–52.
Walawender, M.J., et al., 1990. Origin and evolution of the zoned La Posta-type plutons, eastern Peninsular Ranges batholith, southern and Baja California. In: Anderson, J.L. (Ed.), The Nature and Origin of Cordilleran Magmatism. In: Geological Society of America Memoir, vol. 174. GSA, Boulder, Colorado, pp. 1–18.
Walker, J.C.G., Hays, P.B., Kasting, J.F., 1981. A negative feedback mechanism for the long-term stabilization of Earth's surface temperature. J. Geophys. Res., Oceans 86 (C10), 9776–9782.
Wallace, P.J., 2005. Volatiles in subduction zone magmas: concentrations and fluxes based on melt inclusion and volcanic gas data. J. Volcanol. Geotherm. Res. 140 (1–3), 217–240.
West, A.J., Galy, A., Bickle, M., 2005. Tectonic and climatic controls on silicate weathering. Earth Planet. Sci. Lett. 235 (1), 211–228.
White, A.F., Schulz, M.S., Lowenstern, J.B., Vivit, D.V., Bullen, T.D., 2005. The ubiquitous nature of accessory calcite in granitoid rocks: implications for weathering, solute evolution, and petrogenesis. Geochim. Cosmochim. Acta 69 (6), 1455–1471.
Zachos, J.C., Dickens, G.R., Zeebe, R.E., 2008. An early Cenozoic perspective on greenhouse warming and carbon-cycle dynamics. Nature 451, 279.
Zeebe, R.E., 2012. LOSCAR: Long-term Ocean-atmosphere-Sediment CArbon cycle Reservoir Model v2.0.4. Geosci. Model Dev. 5 (1), 149–166.